Spontaneous Hot Flow Anomalies at Quasi-Parallel Shocks: 2. Hybrid Simulations

N. Omidi[1], H. Zhang[2], D. Sibeck[3] and D. Turner[4]

1. Solana Scientific Inc.
2. University of Alaska, Fairbanks
3. NASA/GSFC
4. IGPP/UCLA

45
46   ABSTRACT
47
48
49   Motivated by recent THEMIS observations, this paper uses 2.5-D electromagnetic hybrid

50   simulations to investigate the formation of Spontaneous Hot Flow Anomalies (SHFA)

51   upstream of quasi-parallel bow shocks during steady solar wind conditions and in the

52   absence of discontinuities. The results show the formation of a large number of structures

53   along and upstream of the quasi-parallel bow shock. Their outer edges exhibit density and

54   magnetic field enhancements, while their cores exhibit drops in density, magnetic field,

55   solar wind velocity and enhancements in ion temperature. Using virtual spacecraft in the

56   simulation, we show that the signatures of these structures in the time series data are very

57   similar to those of SHFAs seen in THEMIS data and conclude that they correspond to

58   SHFAs. Examination of the simulation data shows that SHFAs form as the result of

59   foreshock cavitons interacting with the bow shock. Foreshock cavitons in turn form due

60   to the nonlinear evolution of ULF waves generated by the interaction of the solar wind

61   with the backstreaming ions. Because foreshock cavitons are an inherent part of the shock

62   dissipation process, the formation of SHFAs is also an inherent part of the dissipation

63   process leading to a highly non-uniform plasma in the quasi-parallel magnetosheath

64   including large scale density and magnetic field cavities.

65

66

67

68

69

2

70   **INTRODUCTION**

71

72   Collisionless dissipation processes at the bow shock result in reflection and/or

73 leakage of ions into the upstream region forming the ion foreshock region (Asbridge et

74 al., 1968; Greenstadt et al., 1968;1980; Gosling et al., 1978; Paschmann et al., 1979;

75 Bonifazi et al., 1980a,b). The ion foreshock is populated with a variety of ULF waves

76 (e.g. Russell and Hoppe 1983; Le and Russell, 1992; Greenstadt et al., 1995) with wave

77 vectors towards the sun but carried back by the solar wind in the opposite direction. Both

78 observations and theoretical studies have also established the turbulent nature of the

79 quasi-parallel shocks and the cyclic reformation of the shock front (e.g. Greenstadt et al.,

80 1977, 1993; Russell, 1988, Thomsen et al., 1988, Thomsen et al., 1990a,b; Burgess 1989;

81 Thomas et al., 1990; Winske et al., 1990; Omidi et al, 1990; Scholer et al., 1993). This

82 behavior is thought to be caused by the convection of upstream generated ULF waves

83 into the shock.

84

85   In an accompanying paper, Zhang et al. [2012] use THEMIS multi-spacecraft

86 measurements to identify a new structure at the quasi-parallel bow shock named

87 Spontaneous Hot Flow Anomaly (SHFA). SHFAs and Hot Flow Anomalies (HFAs)

88 exhibit similar signatures in spacecraft time series data that consist of enhancements in

89 density and magnetic field in the outer part and depletions in these parameters in the core

90 which is also associated with increased temperature and deflected solar wind flow.

91 However, while HFAs form due to the interaction of solar wind discontinuities with the

92 bow shock (e.g. Schwartz et al., 1988;1995;2000; Thomsen et al., 1986;1988;1993;

93   Paschmann et al., 1988; Thomas et al., 1991; Sibeck et al., 1998;1999;2000; Lin,

94   1997;2002; Lucek et al., 2004; Omidi and Sibeck, 2007; Facsko et al., 2008; Eastwood et

95   al., 2008; Jacobsen et al., 2009), SHFAs form in the absence of discontinuities. In the

96   past, local and global hybrid (kinetic ions, fluid electrons) simulations have been used

97   successfully to examine the formation and impacts of HFAs at the bow shock (e.g.

98   Thomas et al., 1991; Lin, 1997; 2002 and Omidi and Sibeck, 2007). Motivated by SHFA

99   observations, we have conducted an investigation of the quasi-parallel bow shock using

100   global hybrid simulations. As we demonstrate here, simulations show the formation of

101   copious structures at the quasi-parallel bow shock and foreshock whose time series

102   signatures resemble those of SHFAs presented by Zhang et al. [2012]. The results

103   indicate that SHFAs are an inherent part of the super-critical quasi-parallel shock

104   dissipation processes and result in highly turbulent and non-uniform magnetosheath

105   plasma.

106

107   The structure of the paper is as follows. Section 2 describes the hybrid model used in

108   this study while the simulation results are described in section 3. Section 4 provides a

109   summary and conclusions.

110

111   2. HYBRID SIMULATION MODEL
112
113
114   The main tool of investigation in this study is a 2.5-D (2-D in space and 3-D in

115   currents and electromagnetic fields) global hybrid simulation model used extensively in

116   the past (e.g. Omidi et al., 2004, 2005, 2006, 2009a,b; 2010; Omidi and Sibeck, 2007;

117   Blanco-Cano et al., 2006a,b, 2009, 2011; Sibeck et al., 2008). In electromagnetic hybrid

118 codes, ions are treated as macro-particles and consist of one or more species (e.g.,

119 differing mass, charge, etc.) whereas electrons are treated as a massless, charge

120 neutralizing fluid (see e.g. Winske and Omidi, 1993, 1996).

121

122   The model consists of a dipole inside a sphere whose surface represents the

123 ionospheric boundary. A solar wind type plasma with electron and ion betas (ratio of

124 thermal to magnetic pressure) of 0.3 each and flow speed of 12 V_A (Alfven speed) is

125 uniformly loaded in the system except for the region inside the ionospheric boundary.

126 This plasma is continuously injected from the left hand boundary throughout the whole

127 run. The remaining boundaries remain open for the plasma to leave. Similarly, open

128 boundary conditions are applied for the electromagnetic fields so that excited waves and

129 turbulence in the system leave through these boundaries. The simulation box lies in the

130 X-Z (noon-midnight meridian) plane with X along the solar wind flow direction (Sun-

131 Earth line) and the magnetic dipole moment in the Z direction so that X corresponds to –

132 X_{GSM} and Z corresponds to Z_{GSM}. The simulation box extends 1500 ion skin depths c/ω_p

133 (where c is the speed of light and ω_p is the ion plasma frequency) in the X and Z

134 directions with cell size of 1 ion skin depth. The interplanetary magnetic field (IMF) lies

135 in the X-Z plane and makes a cone angle of 10° with the X axis. To optimize the

136 computational resources, the simulated magnetosphere is smaller (by a factor of ~5) than

137 the Earth's magnetosphere. On the other hand, the simulated plasma parameters and

138 characteristic time and spatial scales such as gyroperiod, or ion skin depth are the same as

139 in the solar wind and magnetosphere. This ensures that the simulations are capable of

140 generating plasma and field values and characteristic scales that can be directly compared

to observations at the Earth's bow shock. As demonstrated in our earlier studies, the physical processes occurring in smaller bow shocks and magnetospheres are similar to those at the Earth's magnetosphere and much can be learned from these simulations including scaling properties of various magnetospheric processes (e.g. Omidi et al., 2004, 2005, 2006, 2009a,b, 2010; Omidi and Sibeck, 2007; Blanco-Cano et al., 2006a,b, 2009, 2011; Sibeck et al., 2008).

3. FORMATION OF SHFAs

Panel (a) in Figure 1 shows the plasma density (normalized to solar wind value) and magnetic field lines in a portion of the simulation domain. The quasi-perpendicular and parallel portions of the bow shock are labeled in this panel with the latter falling primarily in the southern hemisphere. Also labeled is the ion foreshock, upstream of the quasi-parallel shock, and the Foreshock Compressional Boundary (FCB) that separates a highly disturbed and turbulent ion foreshock plasma from a nearly pristine like solar wind that falls inside the ion foreshock (beam) boundary (see Sibeck et al., 2008; Omidi et al., 2009b). Panel (b) in Figure 1 shows the density zoomed around the quasi-parallel shock and the ion foreshock. The latter includes regions of low density labeled foreshock cavitons. The presence of these structures was predicted by global hybrid simulations (Lin, 2003; Lin and Wang, 2005; Omidi, 2007) and confirmed in the ion foreshock (Blanco-Cano et al., 2009, 2011; Kajdič et al. 2010, 2011). Foreshock cavitons are about an R_E (Earth radii) in size and are associated with drops in density and magnetic field in their core by as much as 50% or more and plasma and magnetic field enhancements in

164   their outer edge. They form as a result of the nonlinear evolution of ULF waves and are

165   carried back by the solar wind towards the bow shock. As we show here, the interaction

166   between foreshock cavitons and the bow shock is highly significant and an inherent part

167   of the quasi-parallel shock dissipation processes.

168

169   Although at any given time the structure of the quasi-parallel bow shock is highly

170   turbulent, a closer examination reveals processes that occur at and upstream of the shock

171   on a regular basis. An example of this is illustrated in Figures 2 and 3 that show the

172   density and ion temperature (normalized to solar wind value) respectively at 4 different

173   times (normalized to proton gyroperiod Ω^{-1}) zoomed around the quasi-parallel bow

174   shock. Ion temperature is obtained by calculating the second moment of the velocity

175   distribution function and includes the effects of the energetic ions in the foreshock. Panel

176   (a) in Figure 2 shows a structure at and upstream of the bow shock consisting of density

177   enhancements surrounding a low density region. Examination of panel (a) in Figure 3

178   shows the ion temperature in the low density region is over 600 times hotter than the

179   pristine solar wind. Note that the ion temperature scale in Figure 3 is set to a maximum

180   of 600 for better clarity. This structure looks similar to a simulated HFAs formed at the

181   bow shock due to solar wind discontinuities, e.g. Omidi and Sibeck [2007]. Panels (b)

182   through (d) in Figures 2 and 3 show the time evolution of this structure that penetrates

183   further into the magnetosheath and eventually becomes a part of the highly non-uniform

184   and turbulent magnetosheath. In the process the energetic ions within the structure are

185   injected into the magnetosheath.

186

187   To see the signature of this structure and its time evolution as might be observed

188   in spacecraft data, Figure 4 shows the ion density, total pressure (normalized to solar

189   wind value), velocity (normalized to V_A) and temperature, as well as the magnetic field

190   (normalized to solar wind value) as observed in time at the location marked by "X" in

191   panel (a) of Figure 2. As can be seen, the signature consists of enhancements in density

192   and magnetic field (beginning at time ~250 Ω^{-1}) that reach a factor of ~3 above the solar

193   wind levels. This is followed by large drops in density (minimum value of ~15% of solar

194   wind density) and field (minimum value of ~30% of solar wind magnetic field) in

195   association with flow deceleration and deflection and enhancements in ion temperature.

196   Note that despite the temperature enhancements, the total pressure in the low density core

197   region is below that in the solar wind. Subsequently, the density and magnetic field

198   increase above the solar wind levels by a factor of ~5 before returning to solar wind

199   values. This signature is identical to that of HFAs in general and the SHFAs reported by

200   Zhang et al. [2012]. Given the absence of a solar wind discontinuity in the simulation, we

201   identify this structure as a SHFA.

202

203   To illustrate the formation of this SHFA, Figure 5 shows the total magnetic field,

204   ion temperature and ion velocity in the X direction at two separate times. The top panels

205   show a well developed foreshock caviton upstream of the bow shock. The bottom panels

206   show that the convection of this caviton by the solar wind into the bow shock transforms

207   it into a SHFA. This transformation is associated with further energization of the ions in

208   the core of the caviton and the enhancement of the cavity (reduction in magnetic field and

209   density) which in turn increases the magnetic field and density in the outer parts. The

8

details of the ion velocity distribution functions within the SHFA and their time evolution and their relationship to particle energization process remain to be understood and are under investigation. Preliminary results suggest that ion trapping by the cavitons and also ion reflection between the bow shock and the cavitons may play an important role in the acceleration process. Given the convection of the cavitons towards the bow shock, the back and forth motion of ions between the cavitons and the bow shock can result in particle acceleration through first and second order Fermi processes.

Examination of the simulation results show that SHFAs form regularly along the quasi-parallel bow shock surface as isolated foreshock cavitons, such as that in Figure 5, encounter the shock. We also find that at times, multiple cavitons arrive at the bow shock near simultaneously and result in the formation of larger and more complex structures. An example of this is illustrated in Figure 6 that shows the density zoomed around the quasi-parallel shock at 4 different times. Panel (a) in Figure 6 shows the presence of a number of SHFA like structures along the bow shock that formed at about the same time due to the arrival of multiple foreshock cavitons at the shock. Panels (b) through (d) show the time evolution of these SHFAs as they penetrate into the magnetosheath and result in large inhomogeneities and turbulence in the quasi-parallel magnetosheath.

Figure 7 shows the signature of this event in time series data as observed at points "A", "B", "C" and "D" shown in panel (a) of Figure 6. Density, magnetic field and temperature are normalized to solar wind values and flow speed is normalized to the Alfven speed in the solar wind. The data looks quite different at each observing point. At

point "A", the data shows signatures associated with 2 SHFAs that are shaded. At point "B" two shaded signatures are present that show density and field enhancements and depletions, flow deceleration and the presence of energetic ions and look similar to SHFAs, however, some differences to SHFAs can also be observed. Similarly, at points "C" and "D" signatures similar to SHFAs are present (shaded regions) but clean and full signatures of SHFAs are harder to identify. In effect the presence of multiple SHFAs at the bow shock and their mutual interactions result in highly nonlinear and complex structures whose signatures in spacecraft data would be similarly complex and hard to decipher.

5. SUMMARY AND CONCLUSIONS

Motivated by the multi-spacecraft THEMIS observations of Spontaneous Hot Flow Anomalies at the quasi-parallel bow shock, by Zhang et al. [2012] we have examined the structure of a super-critical quasi-parallel bow shock using global hybrid simulations. The results show the formation of copious structures at the quasi-parallel shock whose time series data resemble those of HFAs and SHFAs. Given the steady nature of the solar wind and the absence of a discontinuity in the simulation, these structures are identified as SHFAs. The formation of SHFAs in the simulation is tied to the convection of foreshock cavitons by the solar wind and their interaction with the bow shock. Foreshock cavitons are structures of the order of ~1 R_E (Blanco-Cano et al., 2009, 2011; Kajdič et al., 2010, 2011) consisting of low density and magnetic field core region populated with energetic ions and an outer layer with increased density and magnetic field strength. Transformation of a caviton to a SHFA is associated with further

257 energization of ions, reductions in density and magnetic field in the core of the cavitons

258 and the enhancements of the density and magnetic field in the outer region. The size of

259 SHFAs in the Z direction is ~50 ion skin depths which is comparable to that of foreshock

260 cavitons and is of the order of 1 R_E which is also comparable to the size of HFAs at the

261 bow shock.

262

263   Foreshock cavitons have been observed under a wide range of solar wind

264 velocities (Mach number) and IMF orientations. During small and intermediate IMF cone

265 angles when the foreshock falls upstream of the dayside magnetosphere, foreshock

266 cavitons are carried by the solar wind into the bow shock. As a result, we expect the

267 formation of SHFAs at the quasi-parallel bow shock over a wide range of solar wind

268 conditions. Although the simulation results shown here correspond to Alfven Mach

269 number of 12 and IMF cone angle of 10º, examination of other runs with lower Mach

270 numbers (down to 6 V_A) and cone angles (smaller than 45º) also shows the formation of

271 SHFAs at the shock. As such, we believe the formation of SHFAs at the quasi-parallel

272 bow shock is a common process and quite significant for ion acceleration and dissipation

273 at the super-critical quasi-parallel bow shock. Similarly, the formation and dissipation of

274 SHFAs as they interact with the bow shock, is critical for determining the properties of

275 the magnetosheath plasma.

276

277   The simulation results also demonstrate that when a number of foreshock cavitons

278 arrive and interact with the bow shock near simultaneously, structures larger and more

279 complex than SHFAs are formed. These structures are influenced by the interaction of the

cavitons with the bow shock but also with each other. As a result, the time series data

obtained at various points along the bow shock are more complex and varied from point

to point and exhibit full or partial signatures of multiple SHFAs. Such interactions also

lead to large inhomogeneities in the magnetosheath. The results presented by Zhang et al.

[2012] and here demonstrate that ion dissipation processes at the quasi-parallel shock are

even more complex than previously thought. Future data analysis and simulations are

needed to shine more light on the impacts of SHFAs on the bow shock, magnetosheath

and the magnetosphere. Similarly, differences between HFAs and SHFAs and their

magnetospheric impacts need to be explored further. The fact that the formation of HFAs

is associated with the presence of solar wind discontinuities while SHFAs form due to the

interaction of cavitons with the bow shock provide a means of distinguishing between

HFAs and SHFAs. For example, Zhang et al. [2012] use the absence of a solar wind

discontinuity associated with an event to identify it as an SHFA. As we learn more about

SHFAs and how they compare and contrast to HFAs other means of distinguishing

between the two may become available.

305 REFERENCES

306 Asbridge, J. R., S. J. Bame, and I. B. Strong (1968), Outward flow of protons from the

307 earth's bow shock, *J. Geophys. Res.*, 73, 5777.

308

309 Blanco-Cano, X., N. Omidi and C. T. Russell (2006a), Macro-Structure of Collisionless

310 Bow Shocks: 2. ULF waves in the foreshock and magnetosheath, *J. Geophys. Res.*, 111,

311 A10205, doi 10.1029/2005JA01142.

312

313 Blanco-Cano, X, N. Omidi, and C. T. Russell (2006b), ULF waves and their influence on

314 bow shock and magnetosheath structures, *Adv Space. Res.*, 37, 1522, doi:

315 10.1016/j.asr.2005.10.043.

316

317 Blanco-Cano, X., N. Omidi and C. T. Russell (2009), Global hybrid simulations:

318 Foreshock waves and cavitons under radial interplanetary magnetic field geometry, *J.*

319 *Geophys. Res.*, 114, A01216, doi:10.1029/2008JA013406.

320

321 Blanco-Cano, X., P. Kajdič, N. Omidi, and C. T. Russell (2011), Foreshock cavitons for

322 different interplanetary magnetic field geometries: Simulations and observations, *J.*

323 *Geophys. Res.*, 116, A09101, doi:10.1029/2010JA016413.

324

325 Bonifazi, C., A. Egidi, G. Moreno, and S. Orsini (1980a), Backstreaming ions outside the

326 earth's bow shock and their interaction with the solar wind, *J. Geophys. Res.*, 85, 3461.

327

328   Bonifazi, C., G. Moreno, A. J. Lazarus, and J. D. Sullivan (1980b), Deceleration of the

329   solar wind in the earth's foreshock region: ISEE 2 and IMP 8 observations, *J. Geophys.*

330   *Res.*, 85, 6031.

331

332   Burgess, D. (1989), On the effect of a tangential discontinuity on ions specularly

333   reflected at an oblique shock, *J. Geophys. Res.*, 94, 472.

334

335   Eastwood, J. P., et al. (2008), Themis observations of a hot flow anomaly: Solar wind,

336   magnetosheath, and ground-based measurements, *Geophys. Res. Lett.*, 35, 332

337   doi:10.1029/2008GL033475.

338

339   Facsko, G., et al. (2008), A statistical study of hot flow anomalies using Cluster data, *Adv*

340   *Space. Res.*, 41 (8), 1286, doi:10.1016/j.asr.2008.02.005.

341

342   Gosling J. T., J. R. Asbridge, S. J. Bame, G. Paschmann, and N. Sckopke (1978),

343   Observations of two distinct populations of bow shock ions in the upstream solar wind, *J.*

344   *Geophys. Res*, 5, 957.

345

346   Greenstadt, E. W., et al. (1968), Correlated magnetic field and plasma observations of the

347   Earth's bow shock, *J. Geophys. Res*, 73, 51.

348

349   Greenstadt, E. W., C. T. Russell, V. Formisano et al. (1977), Structure of a quasi-parallel,

350   quasi-laminar bow shock, *J. Geophys. Res.*, 82, 651.

351

352 Greenstadt, E. W., C. T. Russell, and M. Hoppe (1980), Magnetic field orientation and

353 suprathermal ion streams in the earth's foreshock, *J. Geophys. Res*, 85, 3473.

354

355 Greenstadt, E. W., et al. (1993), The quasiperpendicular environment of large magnetic

356 pulses in Earth's quasi-parallel foreshock: ISEE 1 & 2 observations, *Geophys. Res. Lett.*,

357 20, 1459.

358

359 Greenstadt, E. W., et al. (1995), ULF waves in the foreshock, in *Physics of Collisionless*

360 *Shocks*, ed. C. T. Russell, *Adv Space. Res.*, Pergamon, 71.

361

362 Jacobsen, K. S., et al. (2009), THEMIS observations of extreme magnetopause motion

363 caused by a hot flow anomaly, *J.Geophys.Res.*, 114, doi:10.1029/2008JA013873.

364

365 Kajdič, P., X. Blanco-Cano, N. Omidi, and C. T. Russell (2010), Analysis of waves

366 surrounding the foreshock cavitons, *AIP Conf. Proc.,* 1216, 479, doi:10.1063/1.3395907.

367

368 Kajdič, P., X. Blanco-Cano, N. Omidi, and C. T. Russell (2011), Multi-spacecraft study

369 of foreshock cavitons upstream of the quasi-parallel Earth's bow shock, *Planet. Space*

370 *Sci.*, 59, 705, doi:10.1016/j.pss.2011. 02.005.

371

372 Le, G. and C. T. Russell (1992), A study of ULF wave foreshock morphology, II: Spatial

373 variations of ULF waves, *Planet. Space Sci.*, 40.

374

375   Lin, Y. (1997), Generation of anomalous flows near the bow shock by its interaction with

376   interplanetary discontinuities, *J. Geophys. Res.*, 102, 24265.

377

378   Lin, Y. (2002), Global hybrid simulation of hot flow anomalies near the bow shock and

379   in the magnetosheath, *Planet. Space Sci.,* 50, 577, 2002.

380

381   Lin Y. (2003), Global-scale simulation of foreshock structures at the quasi-parallel bow

382   shock, *J. Geophys. Res.*, 108, 1390, DOI 10.1029/2003JA009991.

383

384   Lin, Y., and X. Wang (2005), Three-dimensional global hybrid simulation of dayside

385   dynamics associated with the quasiparallel bow shock, *J. Geophys. Res.*, 110, A12216,

386   doi:10.1029/2005JA011243.

387

388   Lucek, E. A., et al. (2004), Cluster observations of hot flow anomalies, *J. Geophys. Res.*,

389   109, A06207,doi:10.1029/2003JA010016.

390

391   Omidi, N. (2007), Formation of cavities in the foreshock, in *Turbulence and Nonlinear*

392   *Processes in Astrophysical Plasmas* , Editors D. Shaikh and G. Zank, AIP Conference

393   Proceedings, 932, 181.

394

395   Omidi, N., and D. G. Sibeck (2007), Formation of hot flow anomalies and solitary

396   shocks, *J. Geophys. Res.*, 112, A01203, doi:10.1029/2006JA011663.

397

Omidi, N., K. B. Quest, and D. Winske (1990), Low mach number parallel and quasi-parallel shocks, *J. Geophys. Res.*, **95**, 20,717--20,730.

Omidi, N., X. Blanco-Cano, C. T. Russell and H. Karimabadi (2004), Dipolar magnetospheres and their characterization as a function of magnetic moment, *Adv. Space Res.*, 33, Issue 11, 1996.

Omidi, N., X. Blanco-Cano and C. T. Russell (2005), Macro-structure of collisionless bow shocks: 1. Scale lengths, *J. Geophys. Res.*, 110, A12212, doi:10.1029/2005JA011169.

Omidi, N., X. Blanco-Cano, C. T. Russell and H. Karimabadi (2006), Global hybrid simulations of solar wind interaction with Mercury: Magnetospheric boundaries, *Adv. Space Res.*, doi:10.1016/j.asr.2005.11.019.

Omidi, N., T. Phan, and D. G. Sibeck (2009a), Hybrid simulations of magnetic reconnection initiated in the magnetosheath, *J. Geophys.Res.*, 114, A02222, doi:1029/2008JA013647.

Omidi, N., D. Sibeck and X. Blanco-Cano (2009b), Foreshock compressional boundary, *J. Geophys.Res.*, 114, A08205, doi:10.1029/2008JA013950.

Omidi, N., J. P. Eastwood, and D. G. Sibeck (2010), Foreshock bubbles and their global magnetospheric impacts, *J. Geophys. Res.*, **115**, A06204.

421

422 Paschmann, G., et al. (1979), Association of low frequency waves with suprathermal ions

423 in the upstream solar wind, *Geophys.Res.Lett.*, 6, 209.

424

425 Paschmann, G., et al. (1988), 3-Dimensional plasma structures with anomalous flow

426 directions near the Earth's bow shock, *J. Geophys. Res.*, 93,11279.

427

428 Russell, C. T. and M. Hoppe (1983), Upstream waves and particles, *Space Sci Revs*, 34,

429 155.

430

431 Russell, C. T. (1988), Multipoint measurements of upstream waves, *Adv. Space Res.*, 8,

432 147.

433

434 Scholer, M., M. Fujimoto and H. Kucharek (1993), 2-dimensional simulations of

435 supercritical quasi-parallel shocks- upstream waves, downstream waves and shock re-

436 formation, *J. Geophys. Res.*, 98, 18971.

437

438 Schwartz, S. J., et al. (1988), Active current sheets near the earth's bow shock, *J.

439 Geophys. Res.*, 93,11295.

440

441 Schwartz, S. J. (1995), Hot flow anomalies near the earth's bow shock, in *Physics of

442 Collisionless Shocks*, C.T. Russell Editor, Advances in Space Research, Pergamon, 107.

443

444   Schwartz, S. J., et al. (2000), Conditions for the formation of hot flow anomalies, *J.*

445   *Geophys. Res.*, 105, 12639.

446

447   Sibeck, D. G., et al. (1998), Gross deformation of the dayside magnetopause, *Geophys.*

448   *Res.Lett.* , 25 (4), 453.

449

450   Sibeck, D. G., et al. (1999), Comprehensive study of the magnetospheric response to a

451   hot flow anomaly, *J. Geophy. Res.*, 104, 4577.

452

453   Sibeck, D. G., et al. (2000), Magnetopause motion driven by interplanetary magnetic

454   field variations, *J. Geophys. Res.*, 105, 25,155.

455

456   Sibeck, D. G., N. Omidi, I. Dandouras, and E. Lucek (2008), On the edge of the

457   foreshock: model-data comparisons, *Ann. Geophys.*, 26, 1539.

458

459   Thomas, V. A., D. Winske and N. Omidi (1990), Reforming super-critical quasi-parallel

460   shocks, 1. One- and two-dimensional simulations, *J. Geophys. Res.*, 95, 18809.

461

462   Thomas, V. A., D. Winske, M. F. Thomsen and T. G. Onsager (1991), Hybrid simulation

463   of the formation of a hot flow anomaly, *J. Geophys. Res.*, 96, 11625.

464

465   Thomsen, M. F., et al. (1986), Hot diamagnetic cavities upstream from the earth's bow

466   shock, *J. Geophys. Res.*, 91, 2961.

467

468   Thomsen, M. F., et al. (1988), On the origin of hot diamagnetic cavities near the earth's

469   bow shock, *J. Geophys. Res.*, 93, 11311.

470

471   Thomsen, et al. (1990a), Two-state ion heating at quasi-parallel shock, *J. Geophys. Res.*,

472   95, 957.

473

474   Thomsen, M. F., J. T. Gosling, S.J. Bame and C.T. Russell (1990b), Magnetic pulsations

475   at the quasi-parallel shock, *J. Geophys. Res.*, 95, 957.

476

477   Thomsen, M. F., et al. (1993), Observational test of hot flow anomaly formation by the

478   interaction of a magnetic discontinuity with the bow shock, *J. Geophys. Res.*, 98, 15319.

479

480   Winske, D., N. Omidi, K. B. Quest, and V. A. Thomas (1990), Reforming

481   supercritical quasi-parallel shocks: 2. Mechanism for wave generation and front

482   reformation, *J. Geophys. Res.*, **95**, 18,821.

483

484   Winske, D. and N. Omidi (1993), Hybrid codes: Methods and applications, in *Computer*

485   *Space Plasma Physics: Simulation Techniques and Software*, ed. H. Matsumoto & Y.

486   Omura, Terra Scientific, 103.

487

488   Winske, D., and N. Omidi (1996), A nonspecialist's guide to kinetic simulations of space

489   plasmas, *J. Geophys. Res.*, *101*, 17287.

490

491   Zhang. H., et al. (2012), Spontaneous hot flow anomalies at quasi-parallel shocks: 1.

492   Observations, *J. Geophys. Res.*, submitted.

493
494
495
496
497   FIGURE CAPTIONS
498
499
500   Figure 1. Panel (a) shows the plasma density normalized to solar wind value and marks
501   various parts of the bow shock and the ion foreshock. Panel (b) zooms closer into the
502   foreshock and bow shock showing foreshock cavitons.
503
504   Figure 2. Plasma density normalized to solar wind value at 4 times (proton gyroperiods
505   Ω^{-1}) demonstrating the interaction of SHFA with the bow shock.
506
507   Figure 3. Ion temperature normalized to solar wind value at 4 times demonstrating
508   injection of energetic ions into the magnetosheath by SHFA.
509
510   Figure 4. Time series data showing plasma density, three components of velocity and
511   magnetic field and ion temeperature generated at the point marked by "X" in panel (a) of
512   Figure 2. Density, total pressure, magnetic field and temperature are normalized to solar
513   wind values and velocities are normalized to the Alfven speed in the solar wind. The data
514   shows signatures of a SHFA.
515
516   Figure 5. Total magnetic field, ion temperature and velocity in X direction are shown at
517   two times demonstrating the transformation of a foreshock caviton into a SHFA.
518
519   Figure 6. Plasma density at 4 times showing the evolution of a number of SHFAs as they
520   interact with the bow shock and eventually end up in the magnetosheath.
521
522   Figure 7. Time series data showing the variations of total magnetic field, flow speed
523   along X, ion temperature and density at points A, B, C and D marked in panel (a) of
524   Figure 6. Density, magnetic field and temperature are normalized to solar wind values
525   and flow speed is normalized to the Alfven speed in the solar wind.
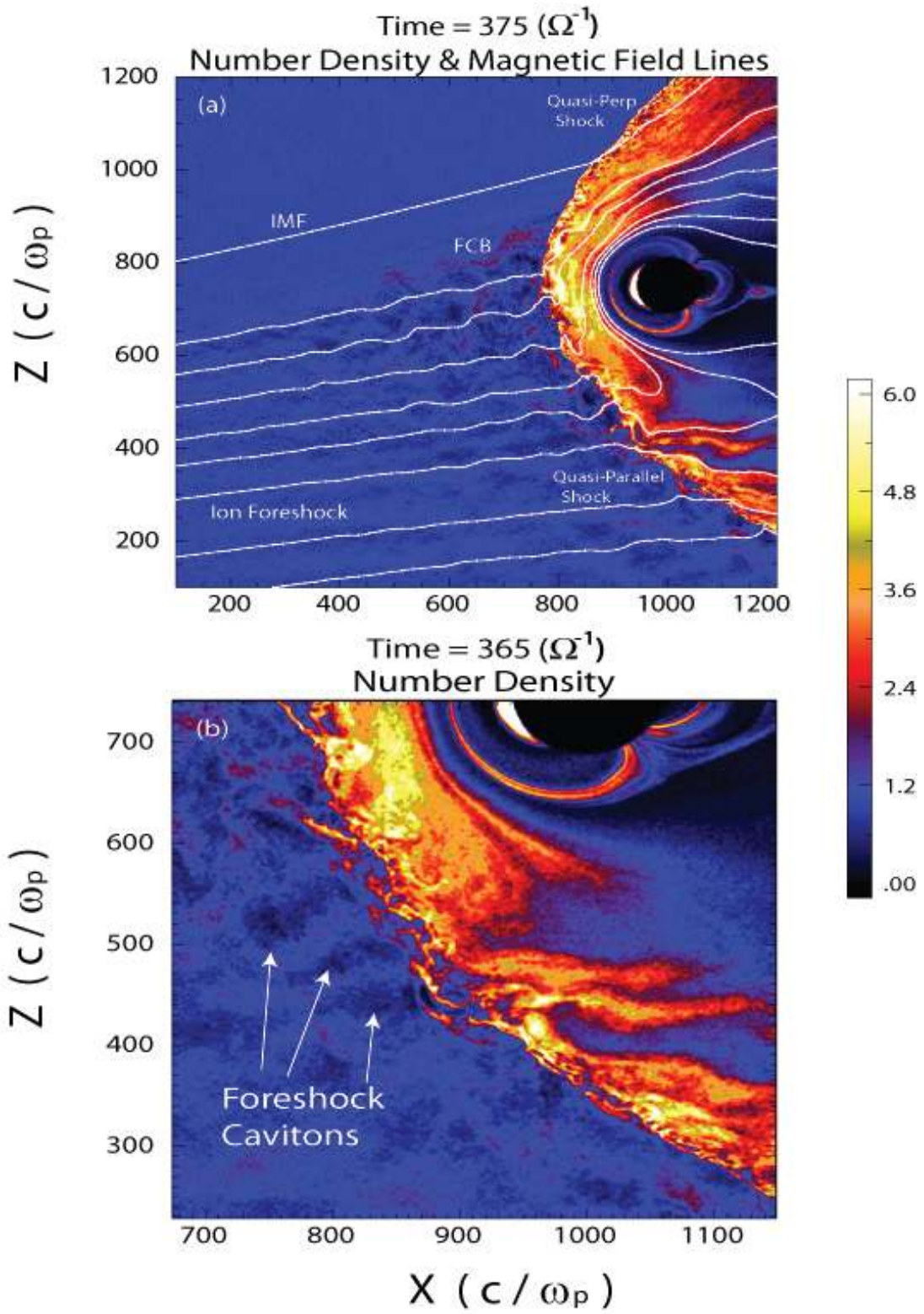526
527
528
529
530
531
532

533
534
535
536
537
538
539
540
541
542
543
544
545
546
547
548
549
550
551
552
553
554
555
556
557
558
559
560
561
562
563
564
565
566
567
568
569
570
571

572
573
574

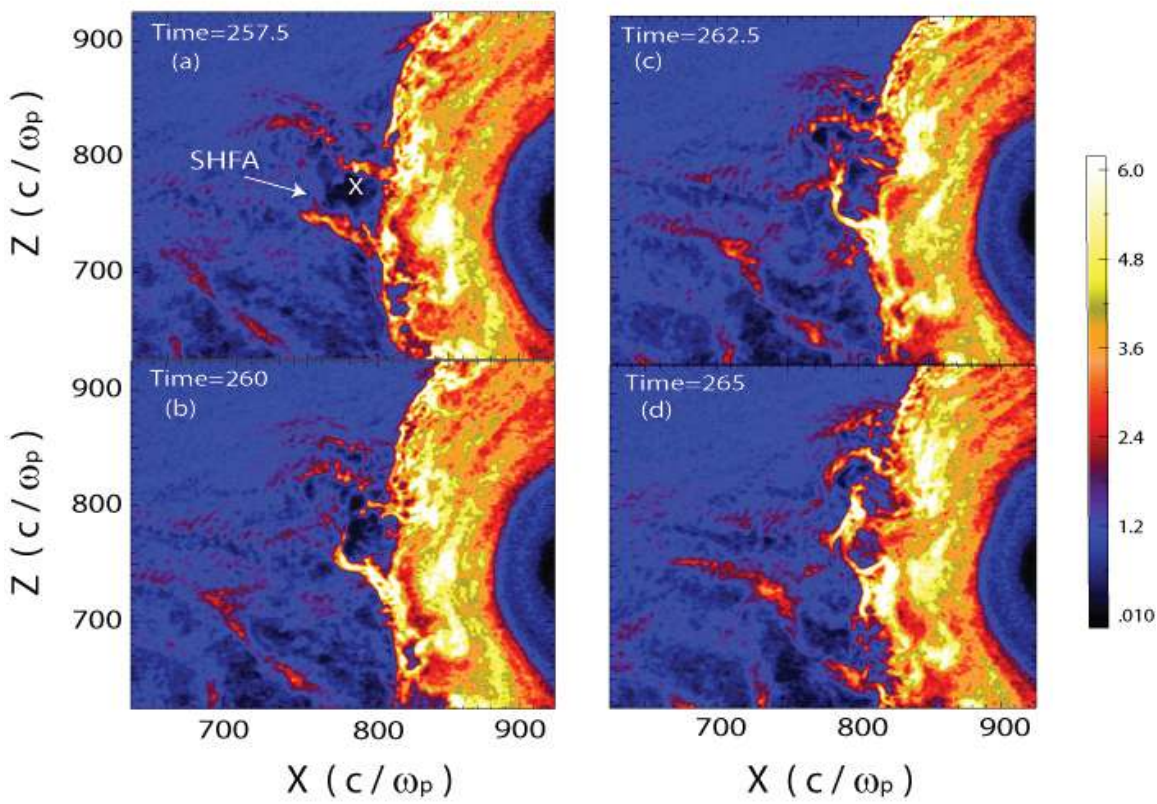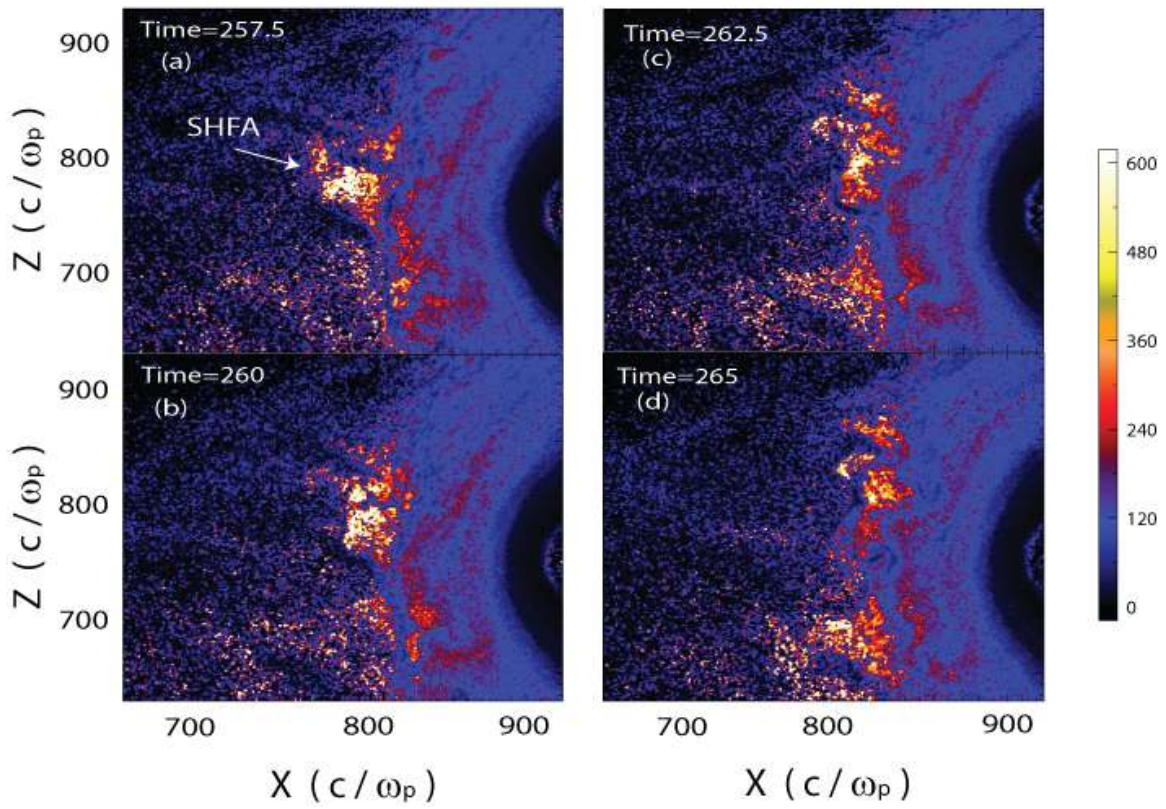Fig. 1

575
576
577
578
579
580

Number Density

Fig. 2

581
582
583
584
585
586
587
588
589
590
591
592
593
594
595
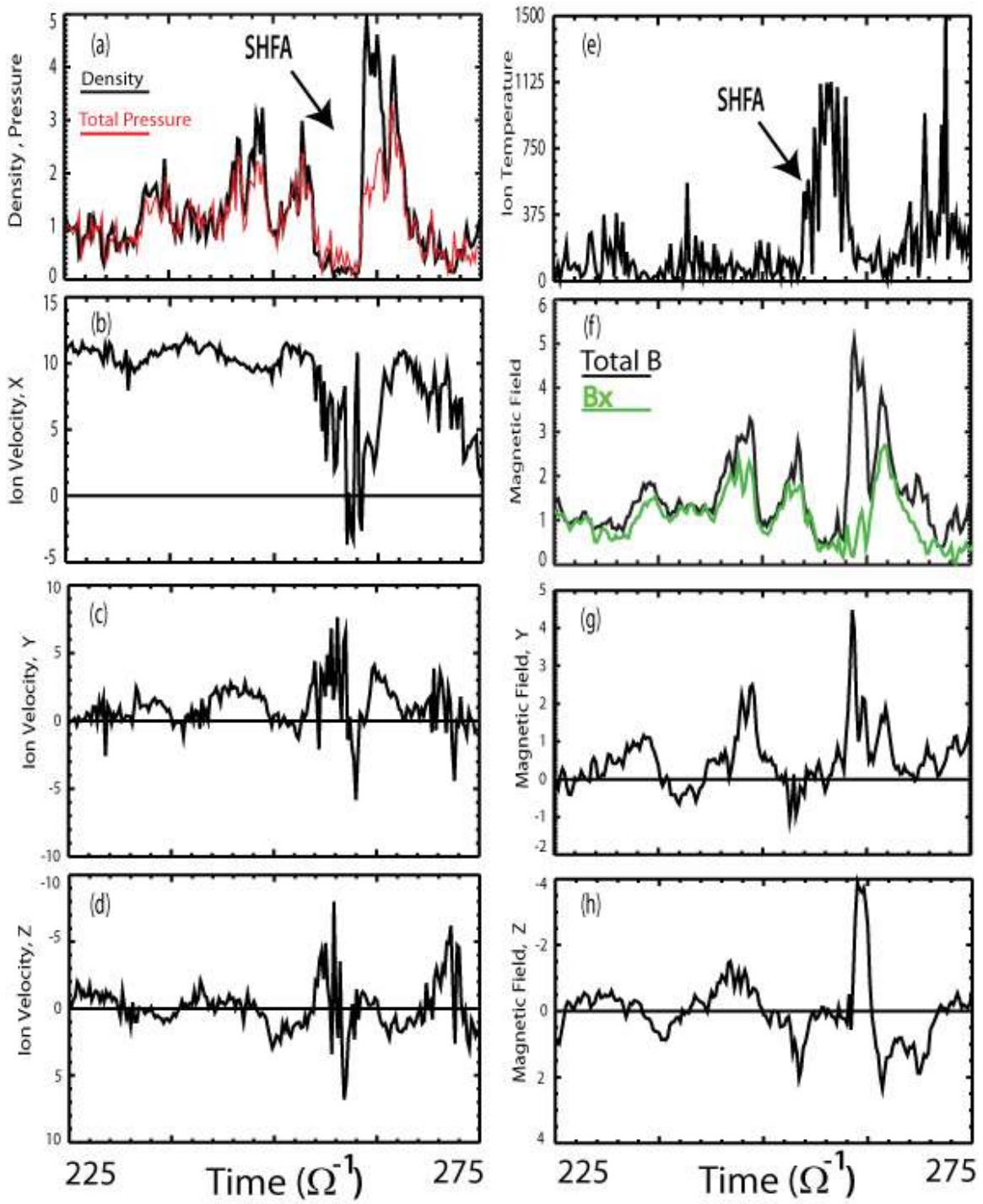596
597

598
599
600
601
602
603

Temperature

Fig. 3

604
605
606
607
608
609
610
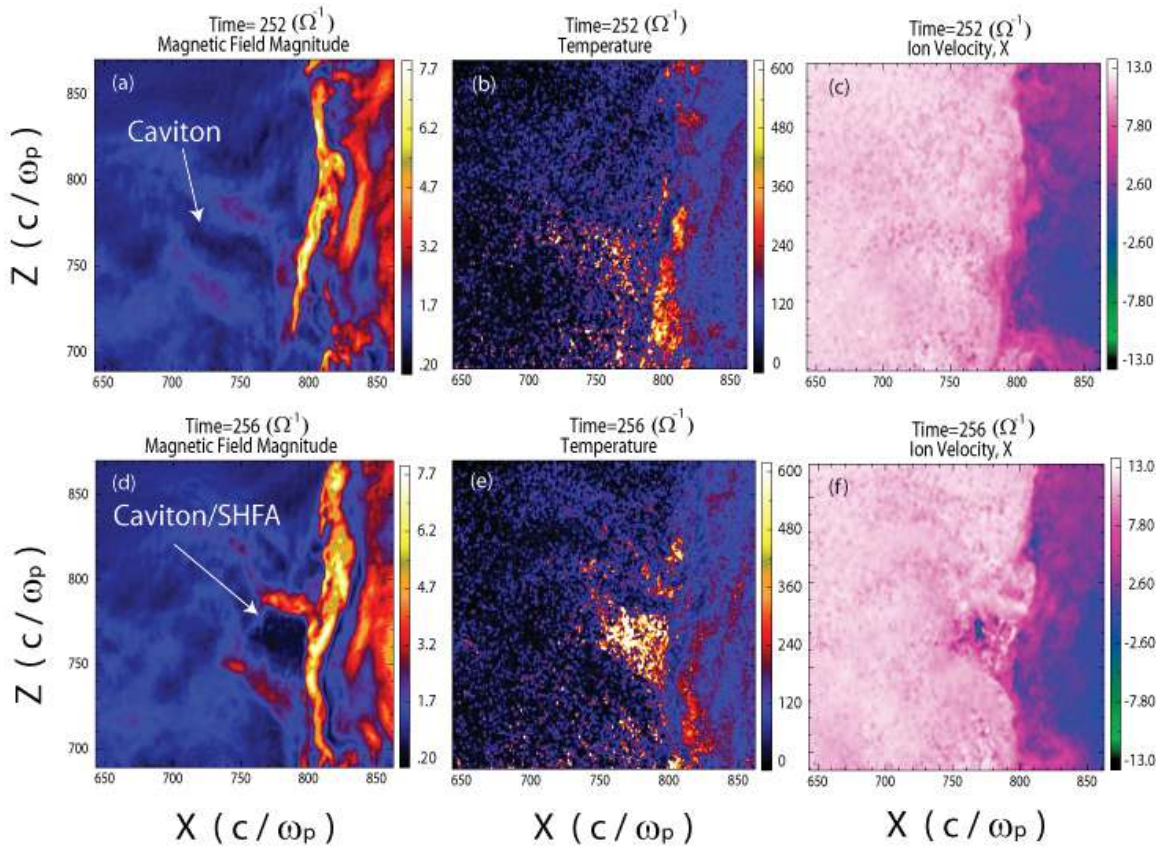611
612
613
614
615
616
617
618
619
620

621
622
623
624

Fig. 4

625
626
627
628
629

25

630
631
632
633
634
635
636
637
638
639
640
641

Fig. 5
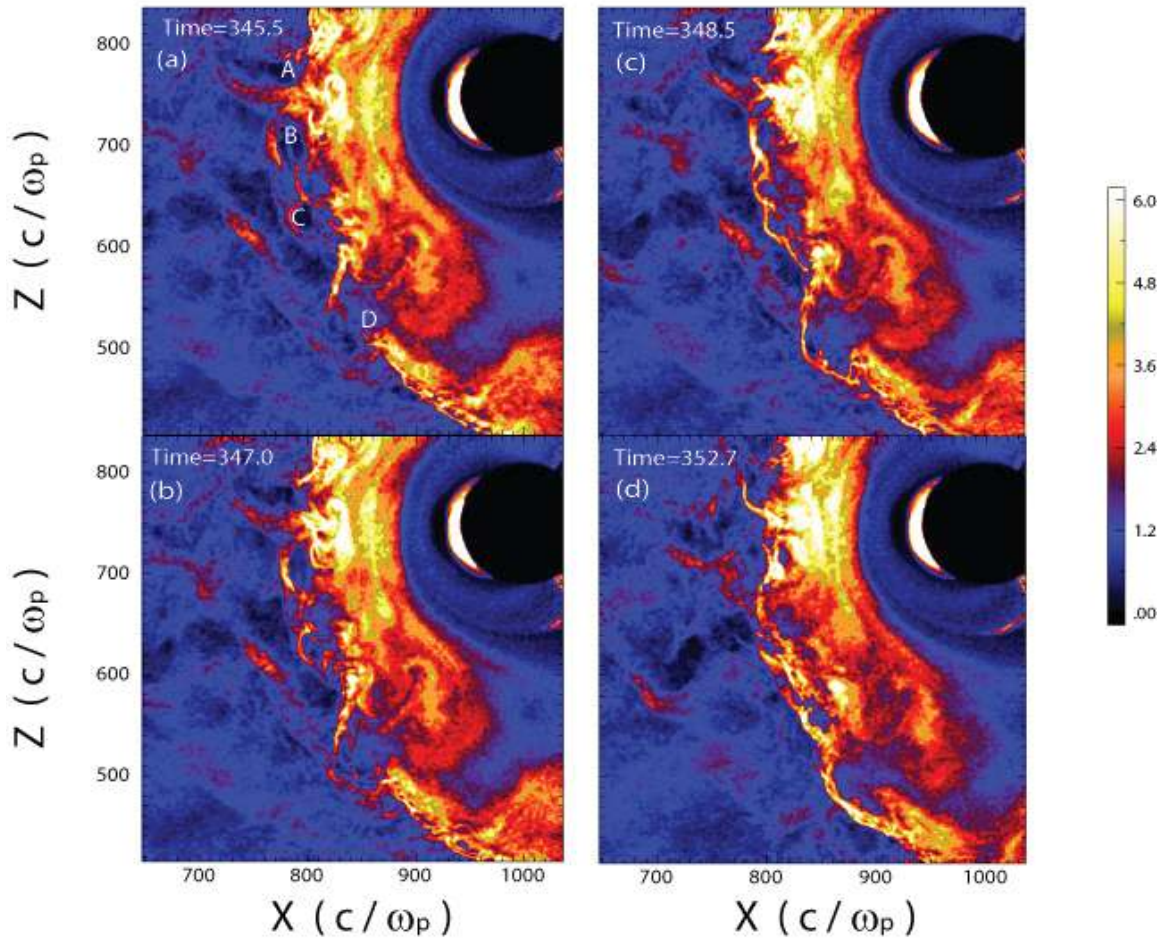
642
643
644
645
646
647
648
649
650
651
652
653

654
655
656
657

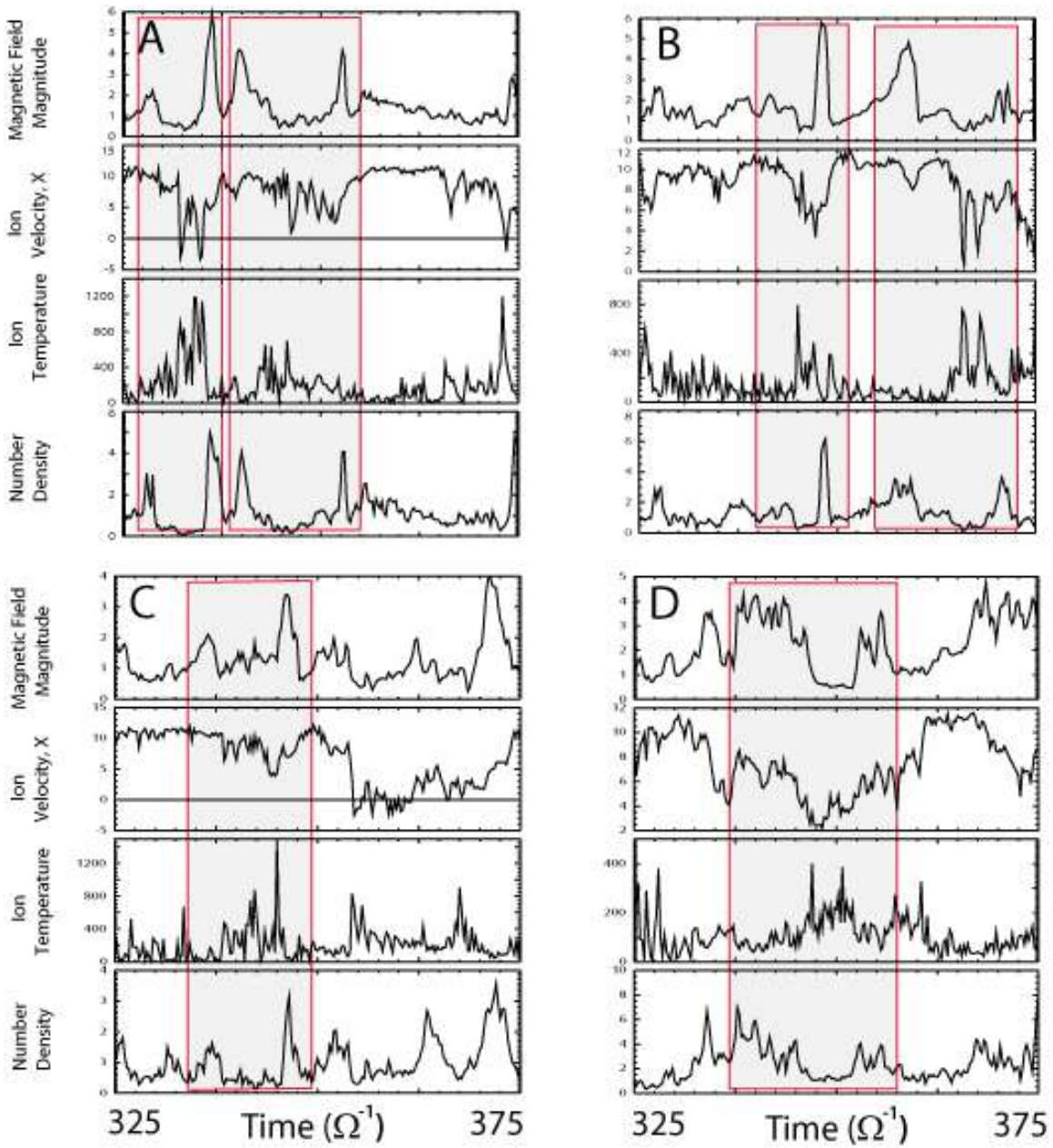# Number Density

658
659
660
661
662
663
664
665
666
667
668   Fig. 6
669
670
671
672
673

674
675
676
677

678
679
680
681
682
683   Fig. 7
684